applied optics

High-absorption optical stack for aluminum kinetic inductance detectors

Zhanzhang Mai,[1] Xucheng Dai,[1] Yingni Chen,[1] Zhongyu Shi,[1] Haoyu Wang,[2,3] Changzhao Pan,[2,3] Xuming Liu,[2,3] Zhao Wang,[2,3] Weijie Guo,[2,3,*] and Yiwen Wang[1,4]

[1]Quantum Optoelectronics Laboratory, School of Physics Science and Technology, Southwest Jiaotong University, Chengdu 610031, China
[2]Shenzhen Institute for Quantum Science and Engineering, Southern University of Science and Technology, Shenzhen 518055, China
[3]International Quantum Academy, Shenzhen 518048, China
[4]qubit@swjtu.edu.cn
*guowj@sustech.edu.cn

Received 18 April 2023; revised 7 June 2023; accepted 7 June 2023; posted 8 June 2023; published 28 June 2023

We present a high-absorption optical stack design for aluminum (Al) kinetic inductance detectors (KIDs). Aluminum can be easily processed in micro-fabrication and is the most conventional superconducting material for KIDs. However, it is challenging to achieve high absorption in the Al absorber because of its high reflection at optical wavelengths. By embedding the thin Al film between an anti-reflection (AR) coating layer and a dielectric-based distributed Bragg reflector, we show that close-to-unity absorption can be achieved around a single wavelength (e.g., ≈98.9% at 1518 nm). The reflection and transmission measurements agree well with the calculation based on the transmission matrix model. We also show our preliminary results of absorption ≥70% in a broader wavelength range (≈230 nm) with multilayer AR coatings. The absorber design in a lumped-element KID is discussed. Our work paves the way to high-efficiency photon-counting and energy-resolving Al-based KIDs in the optical to NIR range. © 2023 Optica Publishing Group

https://doi.org/10.1364/AO.493305

1. INTRODUCTION

Kinetic inductance detectors (KIDs) [1] are superconducting detectors based on high-quality superconducting microresonators [2]. They work on the principle that incident photons can change the surface impedance of the superconducting film due to cooper-pair breaking and kinetic inductance effects. KIDs are easy to fabricate and can be multiplexed into large arrays for sensitive astronomical detections at submillimeter and millimeter wavelengths [3–6]. Because the resonance frequency shift is proportional to the absorbed photon energy and photon number, KIDs also have intrinsic photon-energy-resolving and photon-number-resolving (PNR) capability in the optical to near-infrared (NIR) wavelength range [7–9], which make them attractive in spectrophotometric imaging [10] and quantum applications [11]. In some of these applications, high detection efficiency (DE) close to unity is required, and therefore a sensor with high absorption efficiency is needed.

Optical and NIR KIDs are usually made from disordered superconductors, such as titanium nitride (TiN) [12], hafnium (Hf) [13], and platinum silicide (PtSi) [14]. These films have high resistivity and kinetic inductance fraction, thus giving high response and small pixel size. They also have medium absorption, which is generally below 30% in the NIR wavelength range. To further improve absorption, the optical stack structure has been designed and tested for bulky TiN films at room temperature [15,16]. On the other hand, the Al film is the most conventional material to be processed in micro-fabrication and the Al-based KIDs are well understood. Recently single-photon energy resolution approaching Fano limit has been achieved in a hybrid (Nb, Ti)N-Al KID with the Al film as the photon absorber [7]. We also demonstrate to resolve up to 15 photons using a lumped-element KID made of pure aluminum []. Therefore Al KID can be an alternative choice for PNR and energy-resolving detectors. However, the Al film suffers from very high reflection and low absorption in the optical to NIR wavelength range. As a result, it is a challenge to achieve high efficiency in Al-based KIDs.

In this work, we present an optical stack that is designed to achieve high absorption in the Al film in the NIR wavelength range. In this design, we embed a thin Al film in an anti-reflective (AR) coating layer and a dielectric-based distributed Bragg reflector (DBR) mirror. We perform reflection and transmission measurements on the fabricated optical stacks using a commercial spectrophotometer. The measured results show that close-to-unity absorption at a single wavelength (e.g., ≈98.9% at 1518 nm) and absorption ≥70% in a broader wavelength range (≈230 nm) can be experimentally achieved, which agree well with the calculation based on a transmission matrix model. We also discuss the design of the inductive

absorber in a lumped-element KID optimized for both high absorption and high responsivity.

2. DESIGN AND MODEL

A. Design Principle

For Al-based KID, the thickness of the Al film absorber usually ranges from 10 to 50 nm to boost its sensitivity. Figure 1(a) shows the reflection (R) and absorption (A) of 10 and 50 nm Al film on a lossless Si substrate. In the NIR range, the reflection of 10 nm Al is lower than that of 50 nm Al, but generally is still above 80%. This results in a low absorption (<10%) for both 10 nm Al and 50 nm Al. Even with a lossless quarter-wavelength (QW) SiN_x AR coating layer optimized for 1550 nm, the absorption in the 10 nm Al film is still below 20% at the target wavelength. Therefore the thin Al film must be embedded in an optical stack structure with both AR coating and mirror to achieve high absorption. A superconducting metallic material such as Al is a conventional choice for the mirror but has two problems. First, there will be a finite absorption in the Al mirror, which sets the upper limit of the absorption in the Al absorber; thus it is impossible to achieve close-to-unity absorption under this condition. For example, we study a simple optical stack with a 200 nm Al film as the mirror placed below the 10 nm Al film. We can determine the absorption in both Al films by reformulating the electromagnetic field distribution in terms of Poynting vectors [17]. The calculated results are shown in Fig. 1(b), where we can see the absorption in the Al mirror can reach 20% around 1550 nm when the total absorption is maximized at 1550 nm. Note that the fraction of the absorbed power in the Al mirror will be much smaller (<5%) [16] for a disordered superconductor absorber with lower extinction coefficient. Second, the Al absorber and the bottom Al mirror form a parallel-plate capacitor structure, which will significantly change the properties of the designed KID.

For the above reasons, we choose to use the dielectric-based DBR mirror [18], which consists of an alternating sequence of two different lossless dielectric layers with each layer thickness corresponding to one-quarter of the target wavelength. DBRs with various combinations of dielectric materials have been used in high-efficiency superconducting nanowire single-photon detectors (SNSPDs) [19–21] and transition edge sensors (TESs) [22]. In this work, we select amorphous SiN_x and SiO_2 as DBR materials because they are convenient to fabricate and

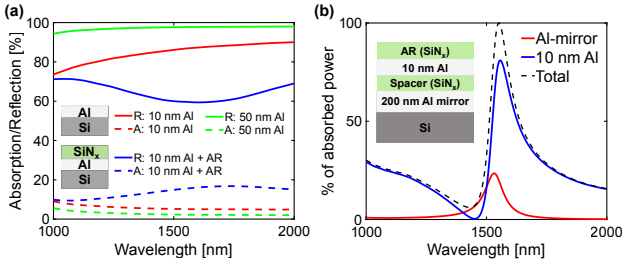

Fig. 1. (a) Calculated absorption and reflection of 10 nm Al film, 50 nm Al film, and 10 nm Al film with a layer of QW AR coating (SiN_x). (b) Calculated absorption with wavelength in the 10 nm Al absorber and 200 nm Al mirror. The total absorption of this optical stack is maximized at 1550 nm. Note that the illustrated structures are not drawn to scale.

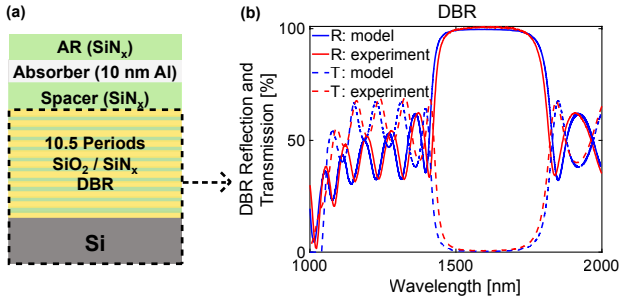

Fig. 2. (a) Illustration of the designed optical stack, which consists of, from top to bottom, AR layer (SiN_x), absorber layer (10 nm Al), spacer (SiN_x), DBR with 10.5 periods of alternating SiO_2/SiN_x layer, and the Si substrate. (b) Reflection and transmission of the 10.5-period $SiO_2/SiNx$ DBR mirror on Si substrate [the dashed box in (a)]: measured reflection (red solid), calculated reflection (blue solid), measured transmission (red dashed), and calculated transmission (blue dashed).

have negligible absorption in the optical to NIR wavelength range. Between the absorber and DBR, we insert a layer of low microwave loss SiN_x [23] as a spacer, which is used to tune the absorption wavelength by varying its thickness. We also use a layer of SiN_x as the AR coating on the top. The whole optical stack design, which is referred to as the "standard structure" in this paper, is illustrated in Fig. 2(a).

B. Transfer Matrix Method

To analyze the absorption in the Al absorber, we use the transfer matrix method [24] to calculate the reflection (R) and transmission (T) of the designed optical stack with K layers. We characterize the jth layer with the thickness d_j and wavelength-dependent complex refractive index $\tilde{n} = n - ik$, where n and k are the refractive index and extinction coefficient, respectively. Considering that the light of wavelength λ is normally incident onto the optical stack in the air, the magnitude of the electric field on top of the first layer E_0 and the transmitted electric field from the bottom of the kth layer E_{k+1} is connected by

$$\mathbf{E}_0 \begin{bmatrix} 1 \\ n_0 \end{bmatrix} = \begin{bmatrix} B \\ C \end{bmatrix} \mathbf{E}_{K+1}, \tag{1}$$

$$\begin{bmatrix} B \\ C \end{bmatrix} = \prod_{j=1}^{K} \begin{bmatrix} \cos\delta_j & i \cdot \sin\delta_j/\tilde{n}_j \\ i \cdot \tilde{n}_j \sin\delta_j & \cos\delta_j \end{bmatrix} \begin{bmatrix} 1 \\ n_0 \end{bmatrix}, \tag{2}$$

where n_0 is the refractive index of air, $\delta_j = 2\pi\tilde{n}_j d_j/\lambda$ is the phase shift across each layer, and $[\,B\;C\,]^{\mathsf{T}}$ represents the corresponding characteristic transfer matrix. Then the reflection and transmission of the optical stack are given by

$$R = \left|\frac{B - C}{B + C}\right|^2, \tag{3}$$

$$T = \left|\frac{2}{B + C}\right|^2. \tag{4}$$

Using Eqs. (3) and (4), we can derive the wavelength-dependent reflection and transmission once we know the optical properties

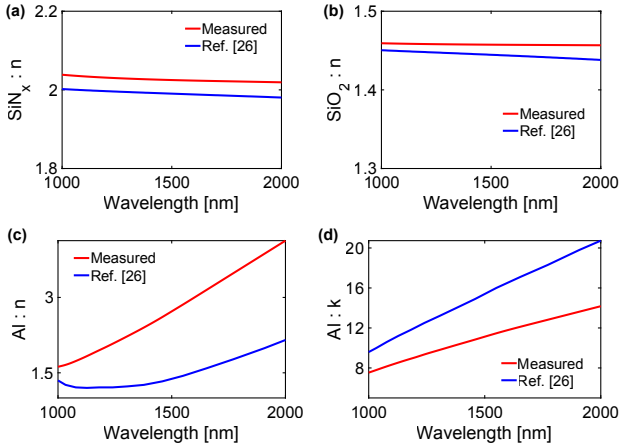

Fig. 3. Optical constants from measurements (red) and Ref. [25] (blue) for (a) SiN_x, (b) SiO_2, and (c), (d) aluminum. In the optical stack design, we use the measured n and k for SiN_x and SiO_2, while choosing to use the n and k from Ref. [25] for Al.

of each layer, and the total absorption of the optical stack is given by $A = 1 - R - T$. This method allows us to optimize the optical stack structure design to maximize the absorption at the target wavelength.

C. Film Characterization

To characterize the optical properties of the SiO_2 and SiN_x film, we deposit a layer of 200 nm thick SiO_2 and SiN_x film on 500 μm double-polished high-resistivity ⟨100⟩ Si substrate, respectively, using the plasma enhanced chemical vapor deposition (PECVD) technique. We perform a room-temperature spectroscopic ellipsometry (Horiba UVISEL) measurement to retrieve the wavelength-dependent complex refractive indices [shown in Figs. 3(a) and 3(b)], which are 1.457 for SiO_2 and 2.024 for SiN_x at 1550 nm. The derived extinction coefficients between 493 nm and 2000 nm are 0, indicating that both SiO_2 and SiN_x have negligible absorption in the optical to NIR wavelength range. As for the single-element layer, the Al film, and Si substrate, we choose to use the values of n and k from Ref. [25] for the optical stack design. However, as will be discussed later, we find the experimental data can be better explained with the measured n and k for the Al film [Figs. 3(c) and 3(d)].

3. MEASUREMENT AND OPTIMIZATION

A. Close-to-Unity Absorption Around 1550 nm

We first design the SiO_2/SiN_x DBR mirror aiming to have total reflection at 1550 nm. The bandwidth $\Delta\lambda$ and reflection R of the DBR can be approximately calculated by

$$\frac{\Delta\lambda}{\lambda_0} = \frac{4}{\pi}\sin^{-1}\left(\frac{n_H - n_L}{n_H + n_L}\right), \tag{5}$$

$$R = 1 - 4\left(\frac{n_L^2}{n_H^2}\right)^p n_L^2/n_{\text{sub}}, \tag{6}$$

where λ_0 is the center wavelength, n_H and n_L are the refractive indices of the high- and low-refractive-index layers at λ_0, n_{sub} is the refractive index of the substrate, and p is the number of stacked pairs (DBR periods). In our case, $n_H = 2.024$ (SiN_x) and $n_L = 1.457$ (SiO_2), with a 10.5-period SiO_2/SiN_x DBR, we expect to have a sufficient reflectivity ≈99.66%, and the stop-band width is ≈270 nm. We fabricate such a 10.5-period DBR on a 3-in Si wafer. The norminal thickness of the deposited SiO_2 and SiN_x layers is 266 nm and 191 nm, respectively, corresponding to one-quarter of the wavelength in the dielectrics. We measure the reflection and transmission of the DBR mirror using a commercial spectrophotometer (PerkinElmer Lamda 750). The results are shown in Fig. 2(b), demonstrating nearly total reflection (≥98%) in a 257 nm wavelength span centered around 1608 nm. The center frequency clearly deviates from 1550 nm, suggesting the uncertainty in micro-fabrication. We think the major uncertainty is the thickness of the SiO_2 layer, which currently cannot be very well controlled. As shown in Fig. 2(b), the experimental results agree well with the model except by changing the SiO_2 thickness from the designed value 266 nm to a fitted value 282 nm.

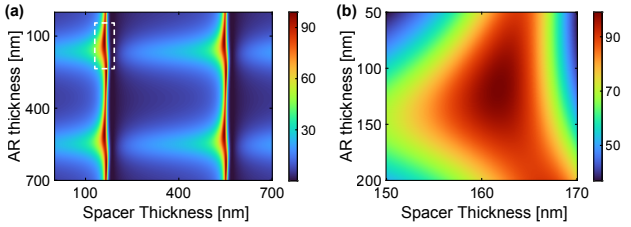

Fig. 4. (a) Calculated absorption of a 10 nm Al film shows periodicity with the AR and spacer thickness. The white dashed-line box marks the first high-absorption area. (b) Enlarged view of the first high-absorption area.

Based on the above DBR, we vary the thickness of the SiN_x AR layer and spacer layer in the range of 1–700 nm with a step of 1 nm, and calculate the corresponding absorption for various thickness combinations. The calculated absorption is shown in Fig. 4, from which we can determine that the optimal optical stack (for 1550 nm) consists of, from top to bottom, 120 nm SiN_x AR coating layer, 10 nm Al absorber layer, 160 nm SiN_x spacer layer, 10.5 periods of SiO_2/SiN_x DBR, and Si substrate. For this optimal design, the absorption in the Al absorber is expected to be over 98% at 1550 nm.

We fabricate a total of five optical stacks by only varying the SiN_x spacer thickness from 100 to 220 nm with a step of 30 nm, including the optimal optical stack with 160 nm spacer. Figures 5(a) and 5(b) present the R/T measurements and the derived absorption of the optimal optical stack in the NIR range from 1000 to 2000 nm. The design shows narrow peaks with close-to-zero reflection and close-to-unity absorption at 1550 nm. However, the experimental reflection and absorption peaks are broadened and shifted to 1627 nm. We find the experimental data can be well explained by the model using the measured n and k [see Figs. 3(c) and 3(d)] for a 10 nm Al film. In the design, we use the n and k from Ref. [25], which should be appropriate for thick Al film but not suitable for the 10 nm Al film in our work. Figure 5(c) shows the absorption peak wavelength with the spacer thickness, where we can see that the peak wavelength can be linearly tuned from 1518 to 1729 nm with a slope of about 1.8 nm peak wavelength shift per 1 nm change

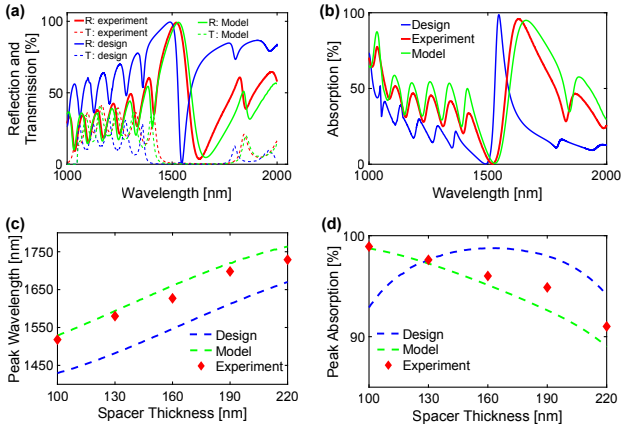

Fig. 5. (a) Reflection (solid line) and transmission (dashed line) of the optimal optical stack, including the experimental data (red curves), the optimal design (blue curves) based on optical constants of Al film from Ref. [25] and norminal SiO_2 thickness (266 nm), and the model (green curves) using measured optical constants of Al film and fitted SiO_2 thickness (282 nm). (b) Absorption of the optimal optical stack. (c) Absorption peak wavelength versus the thickness of the SiN_x spacer. (d) Peak absorption versus the spacer thickness.

in spacer thickness. The measured peak positions agree well with the model but deviate from its designed values by about 82.4 nm on average. This deviation can be reduced by using more accurate optical constants in the design and better controlling the film thickness. Figure 5(d) shows the corresponding peak absorption with the spacer thickness, which also agrees well with the model. It can be seen that ≈98.9% absorption is achieved at 1518 nm for 100 nm spacer thickness.

B. Broadband Absorption

It is not that difficult to achieve high absorption in Al film at a single wavelength. However, the absorption peak wavelength can easily deviate from its designed value due to the uncertainties in the micro-fabrication and film properties; therefore it is better to achieve high absorption in a broader wavelength range. As shown in Fig. 3, the n and k of the Al film change strongly with wavelength while the optical constants of the dielectric layers change slowly. As a result, it is impossible even in principle to achieve high absorption over a wide wavelength range with a single-layer AR coating. This is confirmed by the experimental absorption shown in Fig. 5(b), where we can see a narrow wavelength band (≈130 nm wide around 1627 nm) over which the absorption is above 70%. Therefore a multilayer AR coating is needed for broadband AR. We choose to use the combination of SiN_x and a-Si (amorphous silicon) for AR materials because they have appropriate refraction indices and are relatively easy to fabricate. We also change to use the combination of a-Si/SiO_2 for DBR since a-Si has a higher refraction index (3.383) than SiN_x (2.024) and thus the DBR will have a wider wavelength band with high reflection [see Eq. (6)].

Figure 6(a) shows our preliminary design of the optical stack for broadband absorption, which consists of, from top to bottom, two periods of SiN_x/a-Si AR coating, 10 nm Al absorber, a-Si spacer, 3.5 periods of SiO_2/a-Si DBR, and Si substrate. We optimize the thickness of each layer for high absorption

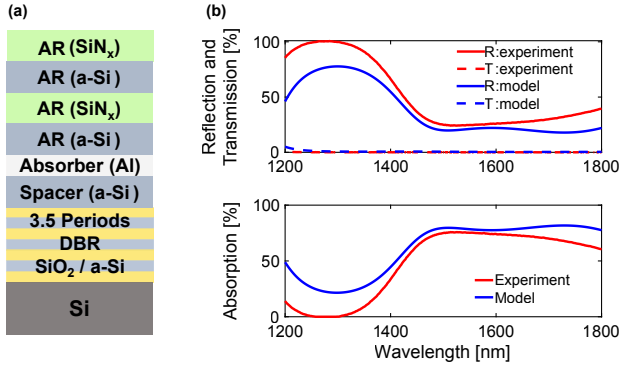

Fig. 6. (a) Designed optical stack for broadband absorption, which consists of, from top to bottom, SiN_x (91 nm), a-Si (172 nm), SiN_x (194 nm), a-Si (51 nm), Al absorber (10 nm), a-Si spacer (78 nm), and a 3.5-period SiO_2/a-Si DBR (266 nm/114 nm). (b) Top, calculated and measured reflection/transmission; bottom, calculated and measured absorption.

between 1450 and 1650 nm. The calculated and measured R, T, and A are shown in Fig. 6(b). Although the design model shows absorption above 70% in the range of 1452–1847 nm, the measured absorption is a bit lower: above 70% in the range of 1470–1700 nm. This indicates that it is indeed difficult to achieve broadband absorption in Al devices. However, this is our preliminary result, and we can make improvements by further optimizing the design.

4. DISCUSSION

In this work, we mainly study the optical stack for a 10 nm Al absorber. However, such a thin Al film may pose a few problems, including a lower quality factor and lower quantum efficiency. Therefore a thicker Al film is favored for a practical device. We vary the Al film thickness and calculate the corresponding maximum absorption at 1550 nm by optimizing the SiN_x AR coating and spacer thickness. The blue curve in Fig. 7(a) shows the maximum absorption as a function of the Al film thickness, where we can see the maximum absorption decreases monotonously with the Al film thickness and drops to below 90% for Al film thicker than 20 nm. To obtain higher absorption for a thicker Al film, one method is to use multilayer AR coatings, i.e., by adding QW SiN_x/SiO_2 layers on top of the standard structure [see Fig. 2(a)]. The orange and yellow curves in Fig. 7(a) show the calculated maximum absorption with Al thickness for extra 1- and 2-period SiN_x/SiO_2 AR coatings. We can see that the absorption drops more slowly since the reflection can be better suppressed with multilayer AR coatings. With a one-period SiN_x/SiO_2 AR layer, the absorption is about 97.7% for 22 nm Al film, which is a practical thickness value. Figure 7(b) shows the maximum absorption of the standard structure at three different NIR wavelengths, suggesting it is easier to achieve high absorption at shorter wavelengths because of the wavelength dependence of k in Al film.

To improve the detection efficiency of a single-pixel lumped-element KID for photon-counting applications [26], we plan to use a fiber optic coupler to focus the incident light onto a spot with diameter ≈20 μm on the absorber. The incident light is generated from a laser diode and transmitted to the fiber

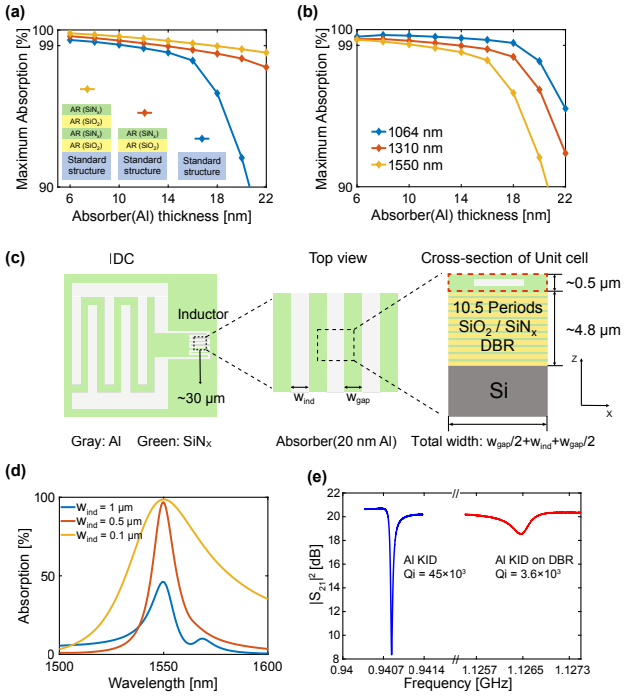

Fig. 7. (a) Calculated maximum absorption at 1550 nm for various Al absorber thicknesses. We compare three designs: the standard structure, and the standard structure with one-period and two-period extra SiN_x/SiO_2 AR coatings. (b) Calculated maximum absorption with Al thickness, by optimizing the standard structure for three different wavelengths. (c) From left to right: sketch of a lumped-element Al KID, meandered Al strip absorber with a filling factor of 0.5 ($w_{ind} = w_{gap}$) in the area where light is focused, and unit cell for simulation. (d) Simulated absorption of the meandered Al absorber with different widths. The absorber is placed in the standard structure optimized for 1550 nm absorption. (e) Measured S_{21} of Al KID at 50 mK with DBR and without DBR.

optic coupler through fibers. In this case, the inductive absorber could be simply designed to be a square of 30 μm × 30 μm, large enough to cover the focused light spot to ensure all incident photons can be picked up. However, this design leads to a lower kinetic inductance and a larger absorber area, which may degrade the sensitivity and the energy resolution. Another absorber design, as illustrated in Fig. 7(c), is using the meandered narrow (submicrometer) inductive strip across the illumination area. This structure will result in a lower refractive index of Al [27], making it possible to achieve high absorption in thicker Al film. We use an EM simulator (Ansys Lumerical FDTD) to simulate the absorption in a meandered 20 nm thick Al absorber that is embedded in the standard optical structure. We take advantage of the absorber symmetry and define a unit cell shown in the far right picture in Fig. 7(c). For simulation, a plane wave source with an in-plane electric field is applied above the top edge of the unit cell, the perfectly matched layer (PML) condition is applied to the Si substrate bottom, and periodic boundary conditions are applied on the left and right edges. We add a mesh override region (red dashed box) around the Al absorber and SiN_x AR/spacer layer, with appropriate mesh steps set as 10 nm and 2 nm along the X (width) and Z (thickness) directions, respectively, to maintain accuracy. We use default mesh accuracy for other regions (DBR and Si substrate). After optimizing the layer thickness for maximum absorption at 1550 nm, we show the simulated absorption for different Al strip widths in Fig. 7(d). We can see that for both 0.1 and 0.5 μm wide Al strips, close-to-unity absorption can be achieved for polarized light at 1550 nm, but the absorption is limited to below 50% for the 1 μm wide Al strip due to the filling factor (= 0.5 in the simulation). This suggests that we can split the 1 μm wide Al strip into ten 100 nm wide nanowires in parallel to improve the absorption. Moreover, we can use other designs to make polarization-independent KIDs [28].

There are a few concerns regarding the feasibility of the above KID design. First, splitting an Al strip into a few parallel nanowires may influence the bifurcation power [29], although the bifurcation power is expected to be unchanged for the same total inductor width. We experimentally tested a resonator with a single 10 μm wide inductor strip and a resonator with four split 2.5 μm wide inductor strips in parallel, and found that the bifurcation powers are the same. However, any anomaly in the width of the nanowires will greatly affect the current density distribution and the bifurcation power. The single-photon response of the KID may also change since the excited quasiparticles can be localized in a single nanowire instead of the full strip. These need further experiments to verify. Second, the presence of a thick DBR (≈4.8 μm) will introduce a significant microwave loss due to the two-level systems (TLSs) [30] in dielectrics. We design a lumped-element Al resonator with an inter-digitated capacitor (IDC) area ≈1mm × 1 mm and a 2 μm wide inductor strip, resulting in a resonance frequency ≈1 GHz. We fabricate this resonator with and without DBR, respectively (both with 50 nm top/bottom SiN_x layers). As shown by the red curve in Fig. 7(e), the measured S_{21} for the whole resonator on top of the DBR has a low internal quality factor ($Q_i \approx 3.6 \times 10^3$). For comparison, the blue curve shows the measured S_{21} for the resonator without DBR. In this case, $Q_i \approx 45 \times 10^3$, indicating that the microwave loss is significantly higher in the presence of thick DBR. To reduce loss, one can place only the inductor on top of the DBR since the TLSs mainly couple to the electric field of the resonator capacitor. However, the thick DBR may cause a height difference of the inductor to the capacitor, which will bring difficulties in device fabrication.

Note that the measurements in this work are performed at room temperature while the KID device works at ultra-low temperature (≈100 mK). The optical constants of each layer may vary when cooling from room temperature to cryogenic temperature, which can be attributed to the thermal-expansion effect and thermal-optical effect. For dielectric layers, such as SiN_x and SiO_2, the magnitude of the thermal expansion coefficients and the thermal-optical coefficients is on the order of 10^{-6} K^{-1} [31–33], indicating that the optical properties of both SiN_x and SiO_2 have little temperature dependence. For the Al film, the thermal expansion coefficient is ≈23.4×10^{-6} K^{-1} at near-room temperature [34], but the residual resistivity ratio (RRR) is measured to be ≈3 [16] at cryogenic temperature, indicating that the conductivity of Al may change greatly from room temperature to cryogenic temperature, which needs further experiments to study.

5. CONCLUSION

In conclusion, we demonstrate a high-absorption optical stack design for Al-based KIDs. We embed a thin Al film absorber between a SiN_x AR coating layer and a SiN_x/SiO_2 DBR mirror, and experimentally show that close-to-unity absorption can be achieved around a single wavelength, e.g., ≈98.9% at 1518 nm. The reflection and transmission measurements agree well with the calculation based on a transmission matrix model. We show our preliminary result of absorption ≥70% in a broader range (≈230 nm) with multilayer AR coating, which increases the bandwidth at the cost of lower absorption. We also discuss the designs of the absorber in a lumped-element KID. Our work demonstrates a promising approach to make high-efficiency photon-counting and energy-resolving Al-based KIDs in the optical to NIR range.

Funding. National Natural Science Foundation of China (61871333, 62001204 , 11904423); National Key Research and Development Program of China (2022YFC2205004); Natural Science Foundation of Sichuan Province (2022NSFSC0518); Basic and Applied Basic Research Foundation of Guangdong Province (2020A1515010864).

Disclosures. The authors declare no conflicts of interest.

Data availability. Data underlying the results presented in this paper are not publicly available at this time but may be obtained from the authors upon reasonable request.

REFERENCES

1. P. K. Day, H. G. LeDuc, B. A. Mazin, A. Vayonakis, and J. Zmuidzinas, "A broadband superconducting detector suitable for use in large arrays," Nature **425**, 817–821 (2003).
2. J. Zmuidzinas, "Superconducting microresonators: Physics and applications," Annu. Rev. Condens. Matter Phys. **3**, 169–214 (2012).
3. J. Hubmayr, J. Beall, D. Becker, H.-M. Cho, M. Devlin, B. Dober, C. Groppi, G. C. Hilton, K. D. Irwin, D. Li, P. Mauskopf, D. P. Pappas, J. Van Lanen, M. R. Vissers, Y. Wang, L. F. Wei, and J. Gao, "Photon-noise limited sensitivity in titanium nitride kinetic inductance detectors," Appl. Phys. Lett. **106**, 073505 (2015).
4. X. Liu, W. Guo, Y. Wang, M. Dai, L. F. Wei, B. Dober, C. M. McKenney, G. C. Hilton, J. Hubmayr, J. E. Austermann, J. N. Ullom, J. Gao, and M. R. Vissers, "Superconducting micro-resonator arrays with ideal frequency spacing," Appl. Phys. Lett. **111**, 252601 (2017).
5. S. Shu, M. Calvo, J. Goupy, S. Leclercq, A. Catalano, A. Bideaud, A. Monfardini, and E. F. C. Driessen, "Understanding and minimizing resonance frequency deviations on a 4-in. kilo-pixel kinetic inductance detector array," Appl. Phys. Lett. **119**, 092601 (2021).
6. M. R. Vissers, J. E. Austermann, M. Malnou, C. M. McKenney, B. Dober, J. Hubmayr, G. C. Hilton, J. N. Ullom, and J. Gao, "Ultrastable millimeter-wave kinetic inductance detectors," Appl. Phys. Lett. **116**, 032601 (2020).
7. P. J. de Visser, S. A. de Rooij, V. Murugesan, D. J. Thoen, and J. J. Baselmans, "Phonon-trapping-enhanced energy resolution in superconducting single-photon detectors," Phys. Rev. Appl. **16**, 034051 (2021).
8. W. Guo, X. Liu, Y. Wang, Q. Wei, L. F. Wei, J. Hubmayr, J. Fowler, J. Ullom, L. Vale, M. R. Vissers, and J. Gao, "Counting near infrared photons with microwave kinetic inductance detectors," Appl. Phys. Lett. **110**, 212601 (2017).
9. B. A. Mazin, S. R. Meeker, M. J. Strader, P. Szypryt, D. Marsden, J. C. van Eyken, G. E. Duggan, A. B. Walter, G. Ulbricht, M. Johnson, B. Bumble, K. O'Brien, and C. Stoughton, "ARCONS: A 2024 pixel optical through near-IR cryogenic imaging spectrophotometer," Publ. Astron. Soc. Pac. **125**, 1348 (2013).
10. S. R. Meeker, B. A. Mazin, A. B. Walter, *et al.*, "DARKNESS: A microwave kinetic inductance detector integral field spectrograph for high-contrast astronomy," Publ. Astron. Soc. Pac. **130**, 065001 (2018).
11. A. E. Lita, D. V. Reddy, V. B. Verma, R. P. Mirin, and S. W. Nam, "Development of superconducting single-photon and photon-number resolving detectors for quantum applications," J. Lightwave Technol. **40**, 7578–7597 (2022).
12. J. Gao, M. R. Vissers, M. Sandberg, D. Li, H.-M. Cho, C. Bockstiegel, B. Mazin, H. G. Leduc, S. Chaudhuri, D. P. Pappas, and K. D. Irwin, "Properties of TiN for detector and amplifier applications," J. Low Temp. Phys. **176**, 136–141 (2014).
13. N. Zobrist, G. Coiffard, B. Bumble, N. Swimmer, S. Steiger, M. Daal, G. Collura, A. B. Walter, C. Bockstiegel, N. Fruitwala, I. Lipartito, and B. A. Mazin, "Design and performance of hafnium optical and near-IR kinetic inductance detectors," Appl. Phys. Lett. **115**, 213503 (2019).
14. P. Szypryt, S. R. Meeker, G. Coiffard, N. Fruitwala, B. Bumble, G. Ulbricht, A. B. Walter, M. Daal, C. Bockstiegel, G. Collura, N. Zobrist, I. Lipartito, and B. A. Mazin, "Large-format platinum silicide microwave kinetic inductance detectors for optical to near-IR astronomy," Opt. Express **25**, 25894–25909 (2017).
15. M. Dai, W. Guo, X. Liu, M. Zhang, Y. Wang, L. F. Wei, G. C. Hilton, J. Hubmayr, J. Ullom, J. Gao, and M. R. Vissers, "Measurement of optical constants of TiN and TiN/Ti/TiN multilayer films for microwave kinetic inductance photon-number-resolving detectors," J. Low Temp. Phys. **194**, 361–369 (2019).
16. K. Kouwenhoven, I. Elwakil, J. van Wingerden, V. Murugesan, D. J. Thoen, J. J. A. Baselmans, and P. J. de Visser, "Model and measurements of an optical stack for broadband visible to near-infrared absorption in TiN MKIDs," J. Low Temp. Phys. **209**, 1249–1257 (2022).
17. O. Deparis, "Poynting vector in transfer-matrix formalism for the calculation of light absorption profile in stratified isotropic optical media," Opt. Lett. **36**, 3960–3962 (2011).
18. X. Ding, C. Gui, H. Hu, M. Liu, X. Liu, J. Lv, and S. Zhou, "Reflectance bandwidth and efficiency improvement of light-emitting diodes with double-distributed Bragg reflector," Appl. Opt. **56**, 4375–4380 (2017).
19. W. Zhang, L. You, H. Li, J. Huang, C. Lv, L. Zhang, X. Liu, J. Wu, Z. Wang, and X. Xie, "NbN superconducting nanowire single photon detector with efficiency over 90% at 1550 nm wavelength operational at compact cryocooler temperature," Sci. China Phys. Mech. Astron. **60**, 120314 (2017).
20. J. Chang, I. E. Zadeh, J. W. N. Los, J. Zichi, A. Fognini, M. Gevers, S. Dorenbos, S. F. Pereira, P. Urbach, and V. Zwiller, "Multimode-fiber-coupled superconducting nanowire single-photon detectors with high detection efficiency and time resolution," Appl. Opt. **58**, 9803–9807 (2019).
21. H. Wang, H. Li, L. You, Y. Wang, L. Zhang, X. Yang, W. Zhang, Z. Wang, and X. Xie, "Fast and high efficiency superconducting nanowire single-photon detector at 630 nm wavelength," Appl. Opt. **58**, 1868–1872 (2019).
22. Y. Geng, W. Zhang, P. Z. Li, J. Q. Zhong, Z. Wang, W. Miao, Y. Ren, J. F. Wang, Q. J. Yao, and S. C. Shi, "Improving energy detection efficiency of Ti-based superconducting transition-edge sensors with optical cavity," J. Low Temp. Phys. **199**, 556–562 (2020).
23. H. Paik and K. D. Osborn, "Reducing quantum-regime dielectric loss of silicon nitride for superconducting quantum circuits," Appl. Phys. Lett. **96**, 072505 (2010).
24. O. S. Heavens, "Optical properties of thin films," Rep. Prog. Phys. **23**, 1–65 (1960).
25. Filmmetric, https://www.filmetrics.com/refractive-index-database.
26. G. Di Giuseppe, M. Atatüre, M. D. Shaw, A. V. Sergienko, B. E. A. Saleh, M. C. Teich, A. J. Miller, S. W. Nam, and J. Martinis, "Direct observation of photon pairs at a single output port of a beam-splitter interferometer," Phys. Rev. A **68**, 063817 (2003).
27. V. Anant, A. J. Kerman, E. A. Dauler, J. K. W. Yang, K. M. Rosfjord, and K. K. Berggren, "Optical properties of superconducting nanowire single-photon detectors," Opt. Express **16**, 10750–10761 (2008).
28. H.-Y. Yin, H. Cai, R.-S. Cheng, Z. Xu, Z.-N. Jiang, J.-S. Liu, T.-F. Li, and W. Chen, "Polarization independent superconducting nanowire detector with high-detection efficiency," Rare Met. **34**, 71–76 (2015).

29. X. Dai, X. Liu, Q. He, Y. Chen, Z. Mai, Z. Shi, W. Guo, Y. Wang, L. F. Wei, M. R. Vissers, and J. Gao, "New method for fitting complex resonance curve to study nonlinear superconducting resonators," Supercond. Sci. Technol. **36**, 015003 (2022).
30. J. Gao, M. Daal, A. Vayonakis, S. Kumar, J. Zmuidzinas, B. Sadoulet, B. A. Mazin, P. K. Day, and H. G. Leduc, "Experimental evidence for a surface distribution of two-level systems in superconducting lithographed microwave resonators," Appl. Phys. Lett. **92**, 152505 (2008).
31. S. Habermehl, "Coefficient of thermal expansion and biaxial Young's modulus in Si-rich silicon nitride thin films," J. Vac. Sci. Technol. A **36**, 021517 (2018).
32. A. W. Elshaari, I. E. Zadeh, K. D. Jöns, and V. Zwiller, "Thermo-optic characterization of silicon nitride resonators for cryogenic photonic circuits," IEEE Photon. J. **8**, 2701009 (2016).
33. J. Gong, R. Dai, Z. Wang, C. Zhang, X. Yuan, and Z. Zhang, "Temperature dependent optical constants for SiO_2 film on Si substrate by ellipsometry," Mater. Res. Express **4**, 085005 (2017).
34. H. M. Otte, W. G. Montague, and D. O. Welch, "X-ray diffractometer determination of the thermal expansion coefficient of aluminum near room temperature," J. Appl. Phys. **34**, 3149–3150 (1963).